INSTITUT DE FRANCE
Académie des sciences

Comptes Rendus
Physique

Alexandre Baron, Ashod Aradian, Virginie Ponsinet and Philippe Barois

Bottom-up nanocolloidal metamaterials and metasurfaces at optical frequencies

Volume 21, issue 4-5 (2020), p. 443-465

Published online: 3 November 2020
Issue date: 16 December 2020

https://doi.org/10.5802/crphys.21

Part of Special Issue: Metamaterials 1
Guest editors: Boris Gralak (CNRS, Institut Fresnel, Marseille, France) and Sébastien Guenneau (UMI2004 Abraham de Moivre, CNRS-Imperial College, London, UK)

Les Comptes Rendus. Physique *sont membres du Centre Mersenne pour l'édition scientifique ouverte*
www.centre-mersenne.org
e-ISSN : 1878-1535

Comptes Rendus
Physique
2020, 21, nº 4-5, p. 443-465
https://doi.org/10.5802/crphys.21

Metamaterials 1 / *Métamatériaux 1*

Bottom-up nanocolloidal metamaterials and metasurfaces at optical frequencies

Nano métamateriaux auto-assemblés opérant en lumière visible

Alexandre Baron [a], Ashod Aradian [a], Virginie Ponsinet [a] and Philippe Barois*, [a]

[a] Univ. Bordeaux, CNRS, Centre de Recherche Paul Pascal, UMR 5031, 33600 Pessac, France

E-mails: alexandre.baron@crpp.cnrs.fr (A. Baron), ashod.aradian@crpp.cnrs.fr (A. Aradian), virginie.ponsinet@crpp.cnrs.fr (V. Ponsinet), philippe.barois@crpp.cnrs.fr (P. Barois)

Abstract. Metamaterials and metasurfaces are artificial composite media engineered to exhibit extraordinary properties of wave propagation. In bulk (3D) metamaterials, such extreme properties may result from non-conventional values of effective homogeneous optical parameters such as the electric permittivity and the magnetic permeability. These features generally originate in the collective response of the constitutive structural elements, which have to be of sub-wavelength dimensions to satisfy the requirement of optical homogeneity, and which have to be highly polarizable to provide efficient optical functions. For visible light applications, sub-wavelength dimensions imply structuration at the nanoscale whereas high polarizability can be achieved by optical resonators such as plasmonic or Mie resonators. Metasurfaces, on the other hand, are 2D equivalent of metamaterials, designed to control the phase, amplitude and possibly polarization of incident EM waves with subwavelength thickness, using interfacial discontinuities effects. This review shows how the bottom-up approach based on nano-chemistry and the self-assembly methods of colloidal physical-chemistry can be used to produce nano-sized tunable magneto-electric resonators which can subsequently be assembled in bulk nanostructured metamaterials as well as in optically thin metasurfaces. Focusing mainly on work carried out at the University of Bordeaux over the past decade, we review some of the optical properties observed in visible light from the fabricated systems. Specific optical experiments and numerical simulations are of crucial importance for the design of the most efficient structures and the extraction of the effective optical parameters.

Résumé. Les métamatériaux et les métasurfaces sont des milieux composites conçus pour posséder des propriétés optiques extraordinaires. Dans le cas des métamatériaux tridimensionnels, les propriétés nouvelles peuvent résulter de valeurs non conventionnelles des paramètres optiques effectifs tels que la permittivité diélectrique et la perméabilité magnétique. Elles proviennent en général de la réponse collective d'inclusions fortement polarisables de dimensions sub-longueur d'onde afin d'assurer une réponse optique homogène. Dans le spectre de la lumière visible, cette contrainte implique une structuration des matériaux à l'échelle nanométrique. Une forte polarisabilité peut être assurée par des résonances optiques plasmoniques ou de Mie.

* Corresponding author.

Les métasurfaces sont les équivalents bidimensionnels des métamatériaux conçus pour contrôler la phase, l'amplitude et si possible la polarisation des ondes transmises ou réfléchies. Cette revue, centrée essentiellement sur les travaux réalisés depuis une décennie à l'Université de Bordeaux, montre comment l'approche dite "bottom-up" fondée sur la nano-chimie et les méthodes d'auto-assemblage de la physico-chimie colloïdale permet de produire des résonateurs magnéto-électriques accordables de dimensions nanométriques et de les assembler pour former des métamatériaux ou des métasurfaces résonants. En parallèle, le développement de simulations numériques et leur association à des mesures optiques spécifiques sont des éléments cruciaux pour la conception des nanostructures les plus efficaces ainsi que l'extraction de leurs paramètres optiques effectifs.

Keywords. Metamaterials, Metasurfaces, Self-assembly, Colloids, Bottom-up, Optical resonances.

Mots-clés. Métamatériaux, Métasurfaces, Auto-assemblage, Colloïdes, Méthode ascendante, Résonances optiques.

1. Introduction

Conceptual notions, such as double-negative materials or artificial magnetic materials, form the backbone of the metamaterials research field. These notions have been available in the literature for decades and the seminal article of V. Veselago is one prominent early attempt [1–4]. However, to materialize, these ideas required modern fabrication techniques capable of effectively manufacturing the envisioned basic units—the so-called *meta-atoms*—and arranging them into a spatially organized ensemble (*metamaterials*).

Early realizations of metamaterials in the microwave range used classical radio-engineering manufacturing techniques, such as printed circuitry. However, for reaching higher operating frequencies, and the visible range, miniaturization to sizes a few tens of nanometers quickly became necessary as the metamaterials community moved toward the visible [5]. Initial designs resorted to *top-down* fabrication: in essence, top-down approaches start from raw pieces of materials that are carved (etched) into the basic units required to generate the desired properties. A classical example of a top-down fabricated meta-atom is the split-ring resonator, lying on a supporting substrate. Etching to the nanoscale with sufficient precision requires state-of-the-art fabrication facilities equipped with nanolithography devices such as electron beams, ion beams, extreme UV, etc. This top-down approach led to spectacular and well-known results [5].

In this review article, we will focus on a radically different range of fabrication methods, known as the *bottom-up* route [6–8]. This designates in reality a wide array of techniques, whereby meta-atoms are synthetized and assembled together from raw, primary materials, and subsequently, arranged spatially into the sought-after meta-structures. In this approach, and for the optical range, meta-atoms are *nanocolloids*, the complexity of which will depend on the desired properties. In physical chemistry, nanocolloids designate a category for microscopic objects with sizes broadly ranging from a few nanometers to a micrometer. They may be solid nanoparticles, aggregates, polymer coils, droplets or vesicles [9, 10]. In the case of metamaterials, the required nanocolloids are most often nanoparticles, or associations of nanoparticles and polymers.

Such a bottom-up approach has become viable only thanks to the extraordinary progress that was witnessed in nanocolloidal engineering and nanoparticle synthesis over the past three decades [6, 11, 12], where the variety of shapes, obtainable geometrical constructs, as well as the variety of usable primary materials (including noble metals and semiconductors) has immensely widened.

Nanocolloids are obtained, in most cases, in the form of a dispersion of a large number of nanoparticles in a liquid solvent; the task of collecting and distributing them into a more or

less dense, well-organized spatial arrangement cannot be done using any means of individual manipulation.[1]

Therefore, only massively *parallel* processes like self-assembly may produce large metamaterials. Self-assembly designates an ensemble of common and highly efficient processes well-known in chemical physics, soft condensed matter physics, and biology, leading to organized two-dimensional or three-dimensional structures of various symmetries. They can either be spontaneous, occurring under the effect of complex—pair or multi-object—interactions, until some free energy is minimized; or they can be directed, i.e. assisted by some external template such as a surface, a host matrix or else guided by external inputs of energy.

There are benefits and drawbacks in using the bottom-up approach compared to the top-down. On the one hand, top-down fabrication provides more precise and reproducible structures that are easily modelled in numerical simulations. This makes it straightforward to optimize and interpret the observed properties. However, samples in most cases are two- or quasi two-dimensional, with limited lateral sizes. Fabrication is time and energy-demanding and requires state-of-the-art, cost-intensive facilities.

On the other hand, the bottom-up approach is often less precise, as disorder is intrinsically introduced with respect to ideal designs, due to the role of thermal energy and entropy in both the synthesis and assembly stages. On the brighter side, chemistry and self-assembly are low-tech, table-top fabrication means, both energy-saving and cost-friendly. They are able to produce materials in greater quantities, making it easier to obtain 3D samples [7, 13, 14].

Globally speaking, it can be stated that the bottom-up routes introduce a trade-off between a lesser structural precision and a better energy footprint.

This review article is devoted to nanocolloidal metamaterials for optics obtained by the bottom-up approach. We will focus especially on the research efforts carried out at the University of Bordeaux over the past decade.

2. Nanocolloidal meta-atoms

As stated in Section 1, the expression *meta-atom* is often used to denote the basic functional element of a metamaterial. Some authors find it confusing since a meta-atom is not an atom (whereas a metamaterial *is* a material). The wording meta-atom nevertheless underlines its indivisible nature shared with true atoms ($\alpha\tau o\mu o\sigma$): the targeted optical function of this element is lost if its structure is broken into separate pieces. We define in the following the meta-atom as the smallest structural element that provides the wanted optical property. Once again, the *meta* prefix implies that the optical response of the meta-atom goes beyond the properties of natural materials. Moreover, anticipating that a metamaterial constructed as a collection of meta-atoms should exhibit homogeneous effective optical parameters, the size of the meta-atoms should be significantly smaller than the operating wavelength. Optical resonators constitute a major class of meta-atoms in which an optical response (e.g. the electric polarizability) exhibits a resonant behavior at some frequency ω_0 in the spectral range of interest. Indeed, the resonance may involve a considerable increase of the optical response upon approaching ω_0 hence leading to extreme values of the effective optical parameters. Moreover, the optical response exhibits a π phase shift upon crossing ω_0 which may lead to counter-intuitive "negative" optical behaviors. A wide set of multipolar electric and magnetic resonances can in principle be excited by the impinging electromagnetic wave. The price to pay is the presence of optical losses imposed by

[1] Indeed, for a volumic (3D) metamaterial operating in the visible, an average density of one to ten active units (nano-resonators) per wavelength will result in a collection of about 10^9 to 10^{12} nanocolloids for a sample with a volume on the order of a cubic millimeter.

causality through the Kramer–Kronig relations. This is a high price that is sometimes overlooked in yet exciting models.

The strategy of the bottom-up approaches to metamaterials reported in this review is to design, synthesize and assemble nanocolloidal meta-atoms exhibiting optical resonances in the visible or near infrared range. The requirement of sub-wavelength dimensions implies that the size of the meta-atoms should lie in the colloidal range from a few tens up to hundreds of nanometers. Two main classes of optical resonators have been proposed and extensively studied in the field of metamaterials, namely plasmonic and Mie resonators.

2.1. *Plasmonic resonators*

In metallic nanoparticles, free electrons oscillate harmonically driven by the electric field of the light wave. When the exciting frequency matches the natural frequency of the electrons in a metallic inclusion, the so-called localized surface plasmon resonance (LSPR) occurs. It is described in a simple way by considering a spherical particle of radius $a \ll \lambda$ and permittivity $\varepsilon_{\mathrm{NP}}$ immersed in a transparent medium of permittivity ε_m, the dipole moment $\mathbf{p}$ induced by the field $\mathbf{E}_0$ of the wave reads

$$\mathbf{p} = 4\pi a^3 \varepsilon_m \frac{\varepsilon_{\mathrm{NP}} - \varepsilon_m}{\varepsilon_{\mathrm{NP}} + 2\varepsilon_m} \mathbf{E}_0. \tag{1}$$

The resonance occurs when the real part of the denominator in (1) vanishes, which is made possible since the real part of the permittivity of the metal is negative below the plasma frequency. The strength of the induced dipole scales as the volume of the particle but the frequency of the LSPR in the dipolar approximation depends solely on the nature of the metal and of the host medium, regardless of the size as long as it satisfies $a \ll \lambda$. LSPR-based systems may indeed accommodate some degree of size-dispersion. For increasing sizes, higher order multipoles come into play and the LSPR red-shifts progressively [15]. Dense materials assembled from plasmonic nanospheres exhibit optical resonances reminiscent of the LSPR resonance of their meta-atoms, but which are generally affected by the electromagnetic coupling between them, as will be shown in Section 3 [16].

A major challenge of the field of metamaterials is the generation of artificial optical magnetism. Early models have suggested that controlling the magnetic response to light would give access to spectacular novel properties like super-lensing, cloaking or light steering by transformation optics [17–19]. The absence of magnetic polarizability in natural materials at visible light and near IR frequencies is well known [20]. Conventional optics indeed assigns the vacuum value μ_0 to the magnetic permeability μ. In 1999 however, Pendry *et al.* suggested that artificial magnetism could be produced by a resonant inductor-capacitor circuit of subwavelength dimension—split ring resonators (SRR)—in which the electromagnetic wave could induce a circular current, thus producing an effective magnetic response [21]. This concept was beautifully illustrated by the observation of negative refraction in microwaves [22]. It was subsequently extended to higher frequencies by reducing the size of the SRR [5], up to visible light frequencies, where the top-down techniques used to engrave SRRs on surfaces reach their limits. Alternative models were then proposed in which the resonant loop that generates the magnetic response is made of a nanoring of plasmonic nanoparticles [23–25]. We shall see in Section 2.2 that colloidal interactions can be used to synthesize 3-dimensional clusters of plasmonic nanoparticles along the models of Figure 1 and measurements of the magnetic response will be presented. The magnetic component of light can also come into play in chiral media. Chirality indeed enables the presence of a magneto-electric coupling within the constitutive relations of a material [26]. Several authors have shown that plasmonic resonances could be used to enhance the optical activity of chiral substances. We mention a few examples of this phenomenon observed in helical clusters of gold

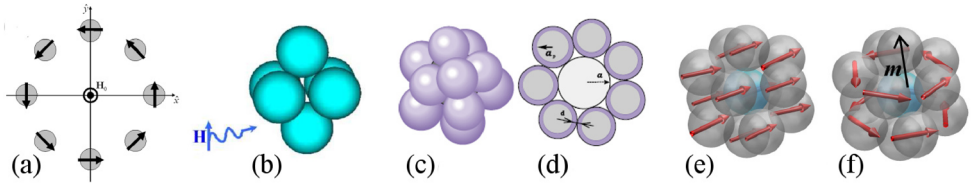

Figure 1. Models of magnetic meta-atoms. (a) Planar model of a ring of plasmonic nanoparticles [23]. (b) Octaedron 3D model [24]. (c, d) Simovski–Tretyakov model of isotropic magnetic nanoclusters [25]. (e, f) Sketch of the electric and magnetic modes in a plasmonic nanocluster [30].

nanoparticles driven by DNA origami, peptide fibrils templates or silica nanohelices obtained by mineralization of self-assembled helices of gemini surfactants [27–29].

2.2. *Mie resonators*

Most nano-antennas and metamaterials were initially designed with plasmonic meta-atoms [5, 31], but it was realized that dielectric meta-atoms could also be used to provide a lot of the functionalities already achieved with plasmonics. To do so, high-index dielectric nanostructures can be built to reach the Mie resonance regime, in which the resonance wavelength will typically be on the order of $n \times a$, where n is the index of refraction of the material and a the typical size of the resonator. As such, a large variety of all-dielectric metamaterials and metasurfaces have been proposed [32–34]. Crystalline silicon that exhibits a large refractive index with low losses for wavelengths above 600 nm is envisioned as a good candidate [35].

In the Mie regime, the scattering of dielectric nanoparticles exhibits electric and magnetic multipole resonances that are described by the coefficients of the vector spherical harmonic expansion of the scattered field under plane wave illumination. For a spherical particle, the electric (magnetic) Mie coefficients a_n (b_n) of order n are given by

$$\{a_n, b_n\} = \frac{\{m,\mu\}\psi_n(mx)\psi_n'(x) - \{\mu,m\}\psi_n(x)\psi_n'(mx)}{\{m,\mu\}\psi_n(mx)\xi_n'(x) - \{\mu,m\}\xi_n(x)\psi_n'(mx)} \tag{2}$$

where ψ_n and ξ_n are the nth order Ricatti–Bessel and Hankel functions of the first kind and are functions of the reduced frequency $x = n_\mathrm{h} kr$. μ is the magnetic permeability of the sphere material (assuming it is 1 for the host medium), n_S and n_h are the indices of refraction of the sphere and the host medium, $m = n_\mathrm{S}/n_\mathrm{h}$, r is the radius of the particle and k is the free-space wavector. The presence of magnetic Mie resonances in the visible spectrum opens the way to optical properties that are not observed in natural materials. A strong magnetic polarizability may indeed lead to yet unknown magnetic bulk materials or to the realization of Huygen's sources exhibiting zero backward scattering.

Nanocolloidal systems enable a tuning of the multipole resonances to achieve a desired optical response. For instance, by carefully tuning the size of a homogenous material with a moderate index of refraction—typically between 1.17 and 2.1—nanoparticles that scatter only in the forward direction can be achieved. This happens because the first order electric and magnetic dipoles resonate at similar wavelengths and with comparable amplitudes. When these resonances overlap perfectly in amplitude and in phase, a so-called Huygens dipole is produced, in reference to the Huygens–Fresnel principle. The concept is the same as the *first Kerker condition*, further detailed in Section 4.2 and occurs whenever $a_1 = b_1$. Zhang *et al.* have demonstrated experimentally direction forward-scattering using Cu_2O nanospheres that were synthesized by

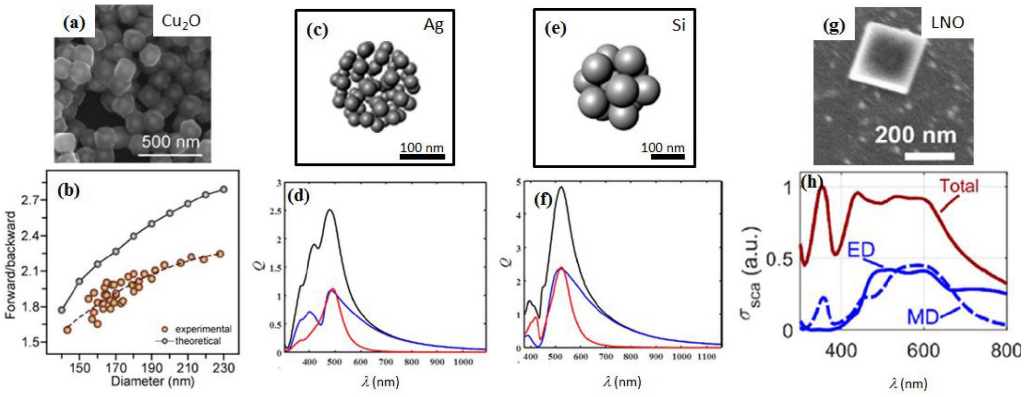

Figure 2. Examples of meta-atoms engineered as Mie resonators. (a) Scanning electron microscope (SEM) images of Copper oxide nanoparticles that exhibit a strong forward-scattering behavior due to their moderate refractive index. (b) Forward to backward scattering ratio as a function of nanoparticle diameter. (a) and (b) are adapted from [36]. (c) Illustration of a 200 nm cluster made of 60 silver nanospheres of diameter $(2r) = 30$ nm. (d) The black line is the total scattering efficiency of the silver cluster shown in (c)—defined as the ratio of the scattering cross-section efficiency to the geometrical cross-section (πr^2)—as a function the wavelength of the exciting field. The blue (red) line is the scattering efficiency due to the electric (magnetic) dipole resonance. (e) Illustration of a dense 13 nanoparticle cluster made of silicon inclusions with diameters of ~80 nm. (f) Same as (d) for the silicon cluster shown in (f). (c), (d), (e) and (f) are adapted from [37]. (g) SEM images of a lithium niobate nanocube for second harmonic generation in NUV. (h) Scattering cross-sections of the nanocube shown in (g) as a function of wavelength. The red line is the total scattering cross-section, the continuous (dashed) blue line is the scattering cross-section of the electric (magnetic) dipole moment. (g) and (h) are adapted from [38].

wet chemistry (see Figure 2 (a,b)) [36]. The concept is not limited to homogenous spheres. As a matter of fact, an effective meta-atom can be produced by clustering inclusions of small resonators that will exhibit a tailored Mie resonance. For instance in [37], Dezert *et al.* have shown theoretically that a cluster of 60 silver nanoparticles will act as a medium exhibiting an effective refractive index that is in the correct moderate range to act as a Huygens dipole (see Figure 2 (c,d)). Furthermore the same authors show that a dense meta-atom made of 13 silicon inclusions constitutes a very efficient Huygens dipole with scattering efficiencies much larger that anything achievable with a hypothetical homogeneous sphere [37] (see Figure 2 (e,f)). It should be noted that the Hugyens dipole concept can be generalized to multipolar systems as forward-scattering occurs whenever $a_n = b_n$ for any order n (see also Section 4.2).

Finally, Mie resonances hold great potential to act as meta-atoms for a variety of applications. A neat example is provided by Timpu *et al.*, who show that lithium niobate (LNO) nanocubes are excellent candidates for second-harmonic generation in the near ultraviolet (NUV) [38]. Indeed, since the energy band-gap is larger than 4 eV, it exhibits low losses in the visible and NUV. Furthermore, LNO has a strong second-order nonlinear susceptibility $\chi^{(2)}$ in those ranges. As a result, by selecting the size of LNO nanocubes fabricated by solvothermal synthesis in the (200 nm–300 nm) range, the authors were able to show SHG emission below 400 nm with giant enhancements compared to bulk LNO due to the Mie resonances of the nanocube (see Figure 2 (g,h)).

2.3. *Loss-compensated resonators and nanolasing*

Meta-atoms described above use resonant schemes in order to provide a significant electromagnetic response. Such schemes go along with resonant losses due to the Kramers–Kronig causality rule. This is even worsened in the often-encountered case of plasmonic resonators in the visible range, where intrinsic Ohmic losses in the metallic parts are already strong [39]. As a result, the obtained resonances are broader and weaker than expected ideally.

One of the strategies to mitigate the losses is to associate optical gain materials to the plasmonic parts in the resonators in what is sometimes called "active plasmonic" designs [40–42]. In the case of plasmonic nanoparticles, it has been shown that resonances can indeed be sharpened, and the associated light emission enhanced, as gain levels are increased [43–45]. Moreover, when gain in the system is increased enough that it exceeds losses, new regimes of spasing and nanolasing are observed; this has been evidenced both in top-down-fabricated structures [41,46] and bottom-up-fabricated ones [46–49].

While experimental realizations for nanoparticle-based nanolasers are still scarce, and investigation mostly relies on full-wave numerical simulations [47], work initiated at the University of Bordeaux was based essentially on theoretical analysis. The studied geometries were either spherical plasmonic nanoparticles immersed in gain, core-shells (with a metal core and active shell), or conversely, nanoshells (with a metal shell and a gain core).

The polarisability α of the particle can be calculated from (1) as $\alpha = p/E_0 = 4\pi a^3 \varepsilon_m (\varepsilon_{\mathrm{NP}} - \varepsilon_m)/(\varepsilon_{\mathrm{NP}} + 2\varepsilon_m)$. When the gain level $\mathrm{Im}(\varepsilon_m)$ is negative (representing a gain material with negative losses) and increased in absolute value (increasing gain), the plasmon resonance is amplified and gradually sharpened [50], or in other terms, the losses in the nanoresonator are compensated. When gain reaches a value such that the imaginary part of the denominator at the plasmon frequency cancels, a singularity of the polarizability appears as the complete denominator vanishes. This was conjectured to be the signature of the onset of spasing/nanolasing [50].

To further investigate the situation theoretically, a detailed electromagnetic description was set up [51]: using an exact Green function formalism, involving individual active emitters randomly aggregated around a metal nanosphere, the equivalent polarizability of the metal-and-emitters system was calculated, composed of the direct response from the metal sphere as well as the contribution arising from the cooperative coupling between emitters and surface plasmons. The analysis was based on an eigenvalue decomposition, where the eigenmodes are coupled, hybrid exciton (from the emitters)-plasmon modes. The calculated optical response of the aggregate indeed showed amplified, loss-compensated plasmon responses as gain was increased. Moreover, when gain levels becomes high enough, sharp peaks corresponding to coherent light emission akin to the Dicke effect were found [51], thereby providing some insight into the physical nature of nanolasing.

In these works, however, as well as in almost all simulation studies on nanoparticle-based nanolasing available in the literature [47], it is implicitly or explicitly assumed that the energy provided by the gain is both stationary in time and independent of the intensity of the nanolasing emission. It is well-known from laser physics that none of these are true in general, as time-dependent regimes may appear (e.g., oscillations) and non-linear effects such as gain depletion occur at high intensity.

A more complete theoretical approach was therefore introduced [52] where the plasmonic response of a homogeneous metal nanoparticle immersed in a sea of surrounding gain elements (dipole emitters) was studied in a space and time-dependent description. The model integrates a quantum formalism (optical Bloch equations) to describe the gain and a classical, fully multipolar treatment for the metal particle. The presence of a lasing threshold was then demonstrated. For gain levels below the lasing threshold, loss compensation takes place and the nanoparticle

plasmon is amplified as usual. For gain above the threshold, a lasing instability sets in: an exponential growth of the emission is initially observed, followed by an energy cascade where all multipolar modes activate. The intricate nonlinear couplings between these modes control the state of emission in the long term.

Recently, the nature of the long-term nanolasing state could be calculated in exact form within the same type of theoretical model, but for a nanoshell geometry, where the core is made of an active material and the shell is a plasmonic metal [53]. For various aspect ratios of the nanoshell, steady-state regimes for nanolasing were demonstrated, with remarkably sharp emission lines with widths as little as 1 nm (and possibly even less with optimization).

In conclusion of this section, situations involving meta-atoms (plasmonic nanoresonators) coupled to optical gain were studied using increasingly elaborate theoretical models. In all cases, a gain level threshold was evidenced, above which lasing in the form of sharp emission lines was found. Below the threshold, plasmon amplification regimes are always found, where the losses of the "natural" resonance of the meta-atom are gradually compensated as the gain level is raised.

3. Metamaterials

In the preceding section, we described several types of nano-resonators which can serve as meta-atoms in the optical wavelength range. In this section, we discuss metamaterials, i.e., materials obtained by assembling such meta-atoms together. We shall present materials made of meta-atoms contained into a host-matrix, as well as materials made of dense packings of only meta-atoms.

Bottom-up techniques can fabricate samples with chemically large numbers of meta-atoms, meaning that they are not restricted to quasi-surfaces, so that 3D bulk materials can be produced. Depending on the specific approach, the actual thickness of the samples can be adjusted from one or a few layers of meta-units up to macroscopic thickness. Therefore, in this section, we will use the formalism of optically-thick materials, such as the optical index, the electrical permittivity and the magnetic permeability. Also, effective-medium approaches will be used to transfer individual meta-atom properties into global, macroscopic ones. This is in contrast with metasurfaces, which will be discussed in the next section, where the optical thickness is small compared to the wavelength.

3.1. *Tunable index of refraction*

Assembling nanocolloidal meta-atoms into 3D (or quasi-3D) materials allows monitoring the optical index. As mentioned before, self-assembly processes intrinsically introduce some degree of disorder or defects, hindering the numerical rendering of the assembled materials. Optical properties are then either fully determined experimentally, or modelled and predicted using somewhat phenomenological effective medium laws.

A very simple situation [54] is a set of spherical plasmonic resonators (14 nm gold nanoparticles), randomly dispersed into a 3D host matrix (a transparent polymer film), see Figure 3 (a). Films of thicknesses ranging from about 40 to 150 nm were obtained by spin-coating aqueous dispersions of gold nanoparticles and polymer onto a silicon wafer, and their optical properties were analyzed using spectroscopic ellipsometry. Due to the plasmonic resonance, the introduction of increasing amounts of gold nanoparticles generates increasing variations in the optical indices of the film. For example, at 6% gold volume fraction, the extracted optical index shows a wide resonance in the visible range, with the refraction index n displaying variations $n = 1.66 \pm 0.13$, see Figures 3(b) and (c).

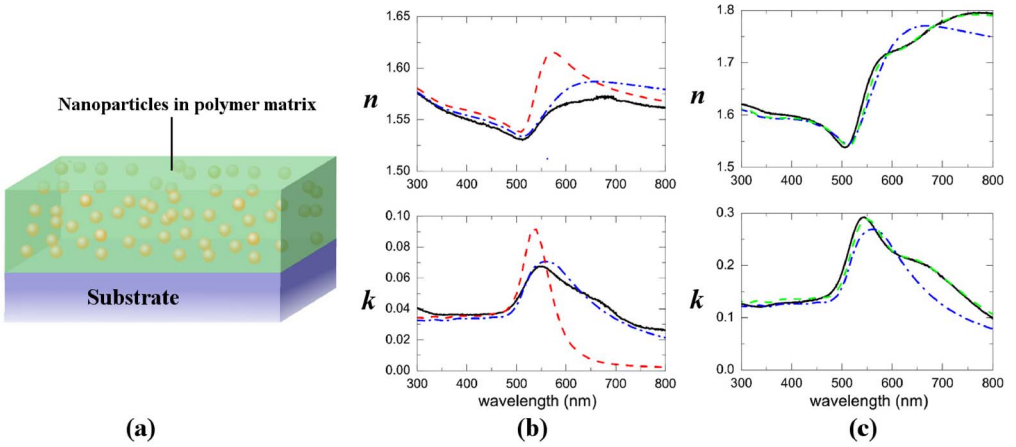

Figure 3. (a) Polymer film with gold nanoparticles [54]. (b, c) Films with 1.6% (b) and 5.7% (c) gold volume fraction. Experimental index of refraction n and extinction coefficient k extracted from ellipsometry (black continuous line). Fits by the classical Maxwell Garnett EMA (red dashed line), by a unimodal ellipsoidal Maxwell Garnett EMA (blue dashed line) or by a bimodal ellipsoidal EMA (green dashed line).

More surprisingly, it was found that even for a low volume fraction of gold nanoparticles ($f \sim 1\%$–5%), the observed plasmonic resonance was affected by electromagnetic coupling between particles, due to disorder and inevitable local inhomogeneities in particle density, which bring some particles close together. As a consequence, even for such dilute systems, the classical Maxwell Garnett Effective Medium Approximation (EMA) failed to predict the measured indices (Figure 3 (b)). Such couplings could be taken into account phenomenologically, using a modified Maxwell Garnett EMA based on a random distribution of ellipsoidal polarizabilities, since couplings can in effect be represented as deformations of the polarizability tensor of individual particles [54], while the nanoparticles actually are and remain spherical. This simple effective model for interparticle couplings proved successful: in simple cases, a unimodal distribution of ellipsoidal polarizabilities was enough to provide reasonably good fits of the experimental data with only two free parameters (Figure 3 (b)). Using bimodal distributions (Figure 3 (c)) made it even possible to reproduce more complex cases where the resonance presented a shoulder in the red; the bimodal population suggested that particles could be categorized into weakly vs. strongly coupled resonators. Such modified Maxwell Garnett EMAs present the advantage of relying on physically meaningful parameters and provide a general tool for the phenomenological description of plasmonic couplings in various disordered nanocomposites, without resorting to advanced (and often impractical) effective-medium theories.

Inhomogeneity in the inter-particle distance can be drastically reduced by encapsulating the plasmonic particles in a unalterable dielectric shell of well-defined thickness. Dense thin films of such core(silver)-shell(silica) nanoparticles were fabricated by several successive Langmuir–Schaefer transfers of a monolayer of nanoparticles at the water–air interface onto a silicon substrate. Their refractive index exhibits a sharp resonant behavior which is nicely reproduced by a single Lorentz oscillator (Figure 4) [55]. Thicker 3D materials can be made by controlled evaporation of a dispersion of plasmonic meta-atoms in microfluidic devices, and the effective refractive index of the final bulk metamaterials can be tuned by controlling the shape, the size and the density of the resonators (Figure 5) [13].

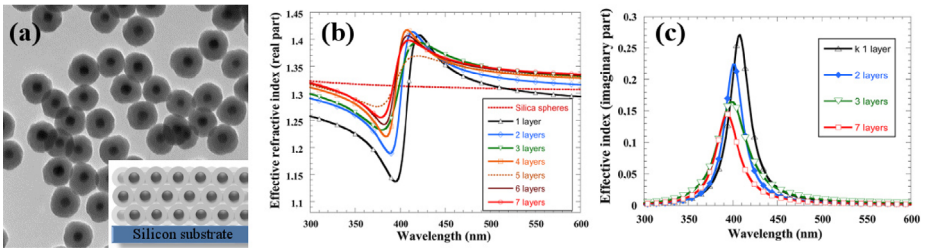

Figure 4. (a) TEM view of core-shell nanoparticles. The diameters of the particle and of the $Ag@SiO_2$ core are 83±4 nm and 27±3 nm respectively. Inset is a sketch of the structure of a 3-layer film deposited on a silicon substrate by the Langmuir–Shaefer technique. (b, c) Plots of the real (b) and imaginary (c) part of the refractive index of metamaterial films as a function of the number of layers (adapted from [55]).

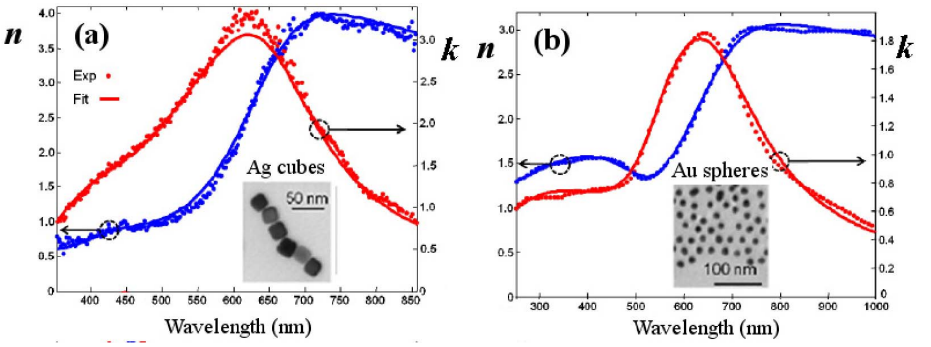

Figure 5. Examples of effective refractive index of 3D composite plasmonic materials made of dense assemblies of silver cubes in (a) and gold spheres in (b). The dots are obtained by direct retrieval from the ellipsometric data, while the continuous lines are a fit to a Tauc–Lorentz model [13].

Although the high volume fraction of metal in self-assembled 3D systems precludes the use of simple mixing rules for the calculation of the effective refractive index, the ellipsometric studies show that the materials behave as homogeneous resonant metamaterials [13].

3.2. *Topological darkness*

The cancellation of the TM reflection from a transparent medium at Brewster's angle is well-known. If losses are introduced via an imaginary part of the optical index, the exact Brewster's extinction disappears. Nevertheless, an exact cancellation of the TM or TE reflection can be reached in thin absorbing films deposited on an absorbing substrate as will be shown below.

For a homogeneous film on a flat surface, the amplitude reflection coefficient of the TM wave is given in standard textbooks

$$r_{\mathrm{TM}} = \frac{r_{\mathrm{TM},1} + r_{\mathrm{TM},2}\mathrm{e}^{2\mathrm{i}\beta}}{1 + r_{\mathrm{TM},1}r_{\mathrm{TM},2}\mathrm{e}^{2\mathrm{i}\beta}} \tag{3}$$

where $\beta = (2\pi/\lambda)N_1 d\cos\phi_1$ is the propagation constant inside the medium, $r_{\mathrm{TM},1(2)}$ is the reflection coefficient from the top (1) and bottom (2) interface, $N_1 = n+\mathrm{i}k$ is the refractive index of the film, d its thickness, λ the wavelength in vacuum and ϕ_1 denotes the direction of the refracted beam within the film. The solutions of the extinction condition display multiple branches shown

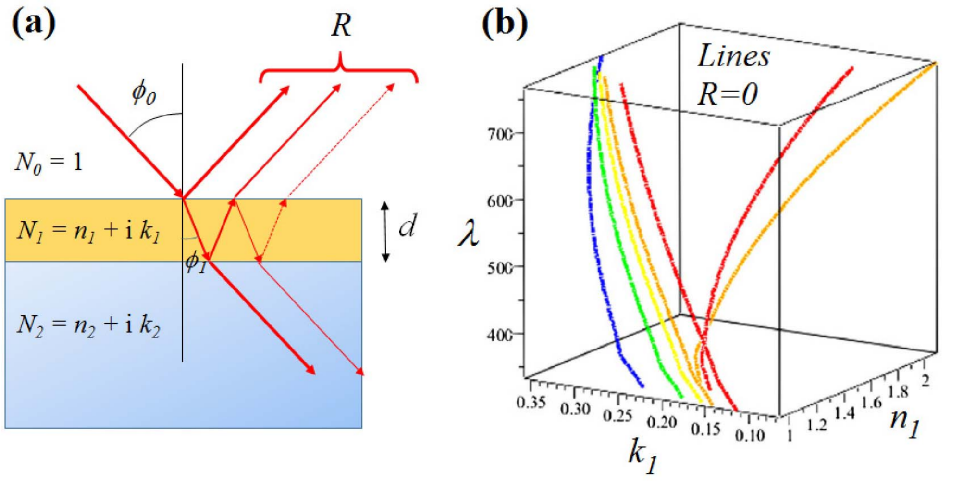

Figure 6. (a) Sketch of the optical geometry. The dark point corresponds to $R = 0$ (destructive interference). (b) Theoretical extinction lines computed numerically for a homogeneous film of index $N_1 = n + ik$ deposited on a silicon substrate at constant angle of incidence $\phi_0 = 50°$ and TM polarization. Colors red, orange, yellow, green and blue correspond, respectively, to thicknesses d of 350, 300, 280, 250 and 200 nm. Note that more than one extinction branch may exist for each thickness (only shown for thicknesses 350 and 300 nm for sake of clarity). Different angles of incidence result in different sets of lines. Similar sets of extinction lines are found for TE polarization (adapted from [56]).

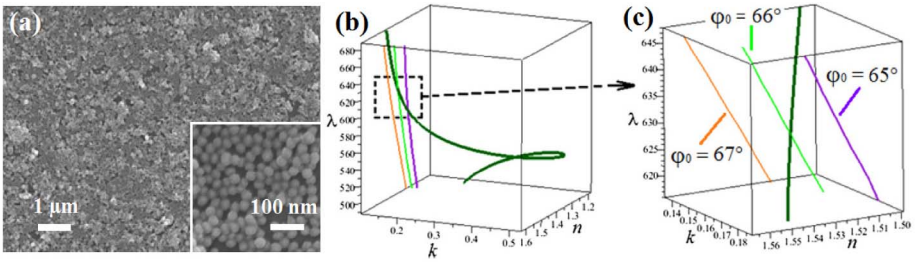

Figure 7. (a) SEM micrographs of a monolayer of core-shell nanoparticles Au(14 nm)@SiO_2(11 nm) transferred on a silicon substrate by the Langmuir–Blodgett technique. (b) 3D views showing the dispersion curve of a 2-layer film of core-shell particles Au(48 nm)@SiO_2(18 nm) (dark green) and the theoretical extinction curves computed for three angles of incidence (AOI). (c) details of the crossing region showing the strong dependence on the AOI. The figure is adapted from [57].

in Figure 6 in (n, k, λ) axes for a particular value of the angle of incidence (AOI = 50°) and for different thicknesses.

A dark point arises when the dispersion curve of a film $(n(\lambda), k(\lambda))$ crosses a line $r_{TM} = 0$. For a film of given thickness on a given substrate, the only experimental parameter is the angle of incidence which must be adjusted to reach the dark point. The existence of the intersection is guaranteed by the Jordan theorem [56]. We illustrate this effect in Figure 7 with experiments carried out on a thin film of core-shell nanoparticles made of a gold core (diameter 14 nm) surrounded by a silica shell (thickness 11 nm) deposited by successive Langmuir–Schaefer transfers onto a

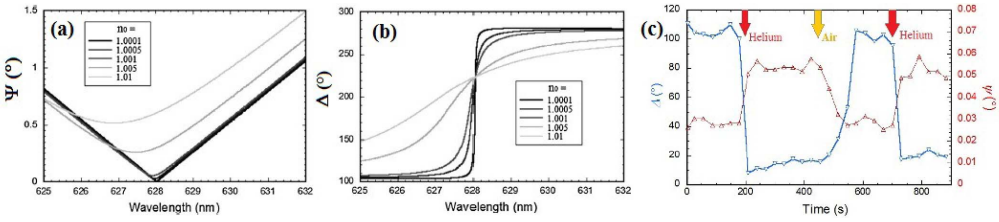

Figure 8. Illustration of the high sensitivity of a plasmonic sensor based on the dark point. The ellipsometric angles Ψ (a) and Δ (right) are computed and plotted for increasing but weak variations of the refractive index of the ambient medium. Note the strong effect on the phase Ψ which provides much higher sensitivity than Δ. (c) Variations of the ellipsometric angles Δ (blue line, left scale) and Ψ (red line, right scale) in the vicinity of the dark point. Helium is injected above the film at $t = 200$ s and $t = 700$ s, air is injected at $t = 450$ s. Note the large variation of $\Delta \sim 100°$ for a change of 2.4×10^{-4} in the refractive index N_0 of the gas. The film is a transparent polymer loaded with 10% vol. gold nanoparticles spin coated on a silicon wafer. The thickness is 179 nm, the dark point is found at AOI = 69.6° and λ = 616 nm.

silicon wafer [57]. A resonant dispersion produces a large exploration of the (n, k) space, which favors the occurrence of the dark condition (see Figure 7), but the presence of a plasmonic resonance is in fact not required to observe a dark point, and it may actually occur either near [58] or away [59] from the resonance, providing in the later case a low-loss phase jump effect.

The dark phenomenon is easily detected by spectroscopic ellipsometry measuring the ratio of the TM to TE reflection coefficients $\rho = r_{\mathrm{TM}}/r_{\mathrm{TE}} = \tan\Psi \mathrm{e}^{-\mathrm{i}\Delta}$. At the dark point, Ψ vanishes and the phase Δ undergoes a sharp jump equal to π. The steep variation of the phase can be exploited for ultra-sensitive sensing [56, 60].

Figure 8 (a,b) illustrates the variation of Ψ and Δ for weak variations of the refractive index of the ambient medium. Figure 8 (c) shows an application to the detection of weak variations of the refractive index of a gas. A phase shift of 100° is observed when air is replaced by helium in the ambient medium above the film. The change in refractive index is 2.4×10^{-4} which yields a sensitivity of the phase on the order of 4×10^5 deg/RIU. Figure 8 (c) shows that a detection accuracy better than 10^{-5} RIU is easily achieved, which is comparable to SPR instruments based on photodiode arrays for instance [61].

This example shows that the total extinction of the reflection due to destructive interferences in a thin absorbing film (topological darkness), similar to the Brewster's extinction on a transparent medium, can be used for sensing with a high sensitivity.

3.3. *3D isotropic optical magnetism*

The magnetism of matter is vanishingly small in natural materials at high frequencies. Paramagnetism and ferromagnetism are slow process that are usually extremely inefficient at frequencies larger than the GHz and diamagnetism typically exhibits magnetic susceptibilities χ_m on the order of 10^{-4} at best. As a consequence, the relative magnetic permeability μ is equal to one for all optical materials in optics and electromagnetism at such frequencies. Natural diamagnetism occurs—in a semi-classical description—because impinging electromagnetic fields induce local polarization currents in atoms or molecules due to circulating charges such as an electron, resulting in an angular momentum that itself produces a magnetic dipole moment **m**. However, these dipole moments are very weak at optical frequencies [20].

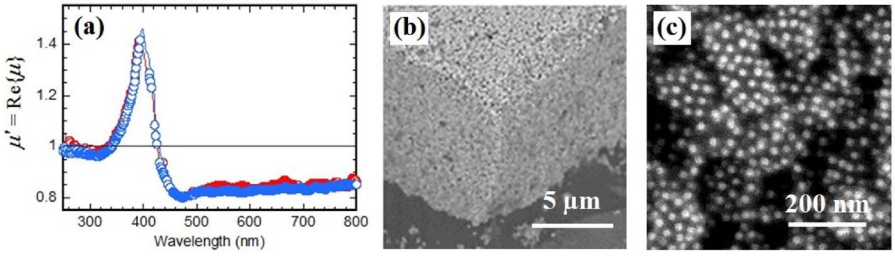

Figure 9. Three-dimensional magnetic metamaterial at optical frequencies. (a) Spectral variations of the retrieved magnetic permeability μ of the metamaterial. (b, c) Scanning electron micrographs of the self-assembled metamaterial at two different scales. Figure adpated from [14].

Plasmonic raspberry systems such as those presented in Section 2.1 (see Figure 1(c–f)) conceptually play the same diamagnetic role as the atom, because circulating plasmonic currents are created that produce an effective magnetic dipole moment near the plasmon resonance wavelength. This resonance wavelength is large compared to the size of the nanosystem [62]. Furthermore, they have pseudo-spherical symmetry, which means that their behavior does not depend on the directions of the electric and magnetic fields incident on the material. As a result, they are ideal to serve as the building blocks of a *three-dimensional isotropic* metamaterial that will exhibit a resonance in the magnetic permeability μ. This contrasts with most realizations of magnetic metamaterials that have been proposed thus far by the *top-down* approach that were mainly two-dimensional and composed of anisotropic meta-atoms [5].

Using a microfluidic evaporation technique aiming at (meta)materials fabrication [13, 63, 64], a three-dimensional metamaterial composed of these raspberries is produced by flowing the solvent containing the colloids through a micro-channel. The solvent eventually evaporates through a semi-permeable membrane and a dense three-dimensional ensemble is molded into the channel. The final metamaterial is truly bulk and constitutes a chunk 100 µm wide, 5 µm deep and several mm long.

For all practical purposes, this means that at optical frequencies the metamaterial may be considered as semi-infinite, and a variable angle spectroscopic ellipsometric analytical retrieval procedure enables the unambiguous determination of the spectral variations of $\varepsilon(\lambda)$ and $\mu(\lambda)$ [14]. The obtained metamaterial reveals a resonant behavior of the magnetic permeability μ with a real part ranging from 0.8 to 1.45 as shown on Figure 9 (a). This corresponds to a magnetic susceptibility comprised between −0.2 and 0.45, three orders of magnitude higher than the highest natural—static—diamagnetic susceptibility. As far as the authors know, this is the first realization of a bulk magnetic metamaterial exhibiting reflexion properties in visible light which are correctly described by an effective isotropic permeability parameter. A tutorial on the direct experimental retrieval procedure is given by Flamant *et al.* [65].

3.4. *Hyperbolic dispersion*

Another type of nanostructures referred to as hyperbolic metamaterials has been proven very promising, as it exploits anisotropy effects to monitor the propagative modes via engineering of the dispersion relation. Indeed, hyperbolic metamaterials present, in some spectral range, two components of the dielectric permittivity tensor ε with opposite signs, as if the material behaved like a metal ($\varepsilon_i < 0$) along at least one direction and like a dielectric ($\varepsilon_j > 0$) along at least another. Because of this extraordinary anisotropy, the isofrequency surfaces open up into

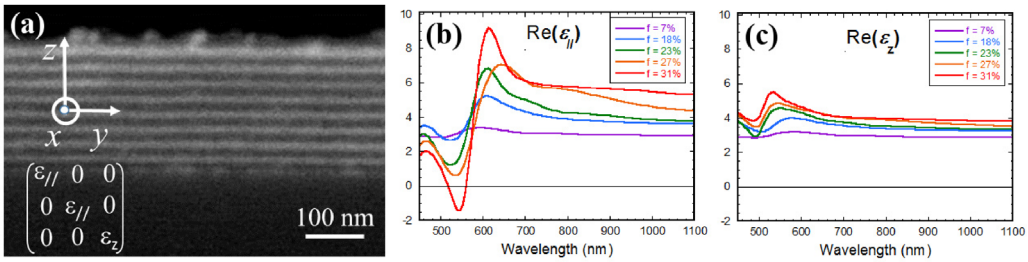

Figure 10. Block copolymer based lamellar metamaterial. (a) Scanning electron micrograph evidencing the regular uniaxial nanostructure. (b, c) Real part of the ordinary and extraordinary permittivities as a function of wavelength for increasing volume fraction f of gold NPs in the lamellae. Figure adapted from [66].

hyperboloids, instead of ellipsoids in a natural material. The extended shape of the isofrequency surfaces allows for propagating waves with large wavevectors, which would be evanescent waves in a natural material. This unique property of propagating high-k waves opens possibilities for imaging with subwavelength resolution. In addition, the phase space volume between two hyperboloids for two values of frequency is infinite, which corresponds to an infinite density of photonic states. Finally, the peculiar dispersion relation gives rise to a number of specific properties, from subwavelength modes to emission engineering, as reviewed in a number of past reports [67–70].

Anisotropic metal-dielectric nanostructures with a hyperbolic dispersion law in the visible wavelength range have been produced with either lamellar stack or cylinder array geometries. Metal-dielectric multilayers are often grown by physical vapor deposition, using either sputtering or evaporation, while cylinder arrays are often produced via the growth of aligned nanowires within porous templating matrices [71] as well as electron beam lithography [72]. As a matter of fact, nanostructuration and anisotropy, along with some degree of long-range order, are spontaneously arising in several self-assembled "soft matter" systems as surfactant organized phases [73], liquid crystals [74], organized nanoparticles, and block copolymers [75]. 3D self-assembly in the form of magnetic NPs chains, induced by the application of an external magnetic field to a ferrofluid, creates a sufficient anisotropy to achieve hyperbolic dispersion laws [76, 77]. Carbon nanotubes packed and aligned by filtration can also constitute hyperbolic metamaterials [78]. Block copolymers present many advantages for the design of anisotropic nanocomposites. They are the result of covalently linking two or more long polymer chains, each called a block, with a chemical nature that can be chosen within a very wide range of chemical functions. Most polymers are incompatible with one another and phase separate in a blend, but because they are covalently linked, distinct blocks of a block copolymer can segregate only as far as the size of the macromolecule, which results in the formation of nanodomains of each block in the solid material. The morphology and degree of order of these nanodomains are fully controlled by the number and relative length of the blocks, while their size directly depends on the whole macromolecule molar mass [79]. By hybridizing an aligned block copolymer nanostructure with gold precursors, Wang *et al.* have produced periodic lamellar stacks of period 28 nm, of alternating layers of pure polymer (dielectric) and layers of composite of polymer loaded with a variable density of 7 nm gold nanoparticles [66]. For large gold loading and close to the plasmon resonance of the nanoparticles, the lamellar stack presents ordinary and extraordinary components of the dielectric function of opposite signs, as evidenced by spectroscopic ellipsometry and shown on Figure 10, demonstrating the potential of this fabrication route for self-assembled bulk hyperbolic metamaterials.

4. Metasurfaces

Metasurfaces are 2D equivalent of metamaterials, designed to control the phase, amplitude and possibly polarization of incident EM waves with subwavelength thickness, using interfacial discontinuities effects (see for instance [80]). Metasurfaces rely on the tailored light scattering of sub-wavelength resonators organized in thin films.

4.1. *Large surfaces*

Just as for 3D assemblies, bottom-up routes for the organization of nano-objects on surfaces rely on constrained hydrodynamics or templating by patterned substrates in order to direct and benefit from self-assembly phenomena, with the major advantage of providing low-cost, large-scale fabrication routes. For instance, dewetting phenomena on topographically patterned substrates have led to silver NPs arrays presenting surface lattice resonance modes [81]. While the size, shape or complex geometry of nanoresonators can tailor their responses, in terms of light absorption and scattering, the relation between these responses and the properties of a metasurface made of the assembled resonators will be computable only if the assembly process results in a surface of good homogeneity. Templating may be a good process to target such homogeneity. A combination of lithography-based topographically patterned substrates and confined drying conditions of a colloidal suspension can lead to well-controlled 2D assembly [82] as demonstrated for instance by an anisotropic appearance in the far-field in the case of aligned nanorods [83]. Templating can also be performed using low-tech wafer-wide spin-coated block copolymer thin films (<50 nm). They constitute chemically patterned substrates, on which metal or dielectric nano-objects can be attached [84] or grown [85–88]. They can also be used as nanometric masks for lithography-like fabrication methods [89, 90]. At the University of Bordeaux, such large scale block copolymer thin films have been used to produce tunable gold nanoresonators in fingerprint-like structures illustrated in the Figure 11, insuring a global azimuthal isotropy together with inter-particle distance homogeneity [86]. The tunable aspect ratio of the resonators strongly affects the optical response of the surface nanostructure on a silicon substrate. Indeed, a description of the optical properties of the samples was derived from ellipsometry data in reflection in terms of an effective optical index, even though the index of so thin films may not be defined independently of the measurement conditions [91,92]. In Ref. [86], increasing the in-plane aspect ratio of the nanoresonators to 2, while keeping the nanostructure thickness constant, was achieved by tuning a simple fabrication process parameter and led to an increase of the index up to 3.2, against ∼1.6 for a nanostructure with same gold density and resonators of aspect ratio 1.

4.2. *Flat optics*

The recent surge in metasurfaces has shown that it is possible to conceive a wide variety of flat optical components that operate thanks to the careful engineering of the amplitudes and phases of the fields scattered by individual resonant objects [34,93]. Bottom-up nanocolloidal routes can play a role here notably thanks to the large amounts of nanoresonators they can produce and the vast surfaces that can be coated by various self-assembly techniques. The variety of meta-atoms that can be synthesized makes it possible to tailor the resonances of the electric dipole moment ($\mathbf{p}$) as well as the magnetic dipole moment ($\mathbf{m}$) both in amplitude and in resonance wavelength.

For instance, when a particle has the property that $|\mathbf{p}| = |\mathbf{m}|$, the so-called *first Kerker condition* is reached and a Huygens dipole is produced [94]. The Huygens dipoles emit spherical waves solely in a direction $\mathbf{u}$ such that $(\mathbf{u}, \mathbf{p}, \mathbf{m})$ forms a direct trihedron. This dipole is named after

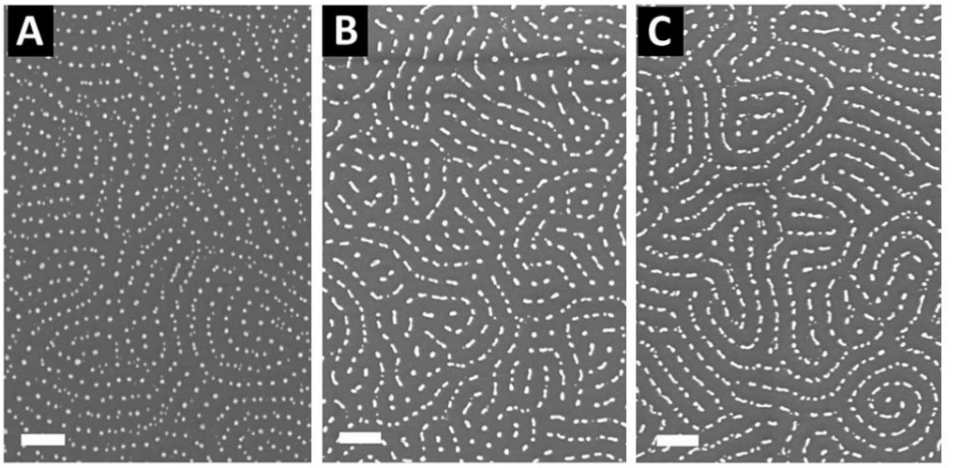

Figure 11. SEM images of gold nanoparticle arrays formed on a silicon wafer using a PS-b-P2VP block copolymer template by immersion in a 1 wt% aqueous gold precursor solution for (A) 1 h, (B) 48 h and (C) 120 h [86]. Scale bars = 100 nm.

Christiaan Huygens as it corresponds to the fictitious point sources of secondary spherical wavelets from the Huygens–Fresnel principle [95]. As a result, when the meta-atom is excited by an impinging plane wave, scattering only occurs in the direction of the exciting wave. This means that a surface composed of these meta-atoms are reflection-less and exhibit a transmission close to unity, these are Huygens metasurfaces [96]. Furthermore the fact that both dipolar resonances are super-imposed means that a full range of dephasing is accessible on the $[0, 2\pi]$ interval and virtually any wavefront may be shaped and flat optical components may be produced, such as prisms or lenses. Huygens sources can be obtained with several systems such as those described in Section 2.2, by exploiting the Mie resonances of homogenous nanoparticles that have the right dispersion and size to reach the Huygens regime, or else by using the clusters system proposed by Dezert *et al.* [37]. It was demonstrated that clusters of plasmonic or dielectric inclusions were good candidates to produce flat lenses and prisms [97]. This 2π phase-shift occurs over narrow-spectral ranges and as a result group-velocity dispersion may be large. This potentially means that metasurfaces composed of isotropic Huygens sources could be used for temporal pulse shaping as was proposed by Decker *et al.* [96] in the case of a periodic metasurface. But since ordering does not play a role, disordered metasurfaces could be used and this is adapted to the bottom-up platform.

Additional types of flat optical components such as filters may be produced. The cases of resonant perfect absorbers is discussed below.

4.3. *Perfect absorbers*

In many circumstances, it may be useful to have a material that absorbs all of the incoming radiation. This concept is certainly applicable to photovoltaics or even some classes of sensors for instance. Furthermore, Kirschoff's law of thermal radiation roughly states that the emissivity of a body is equal to its absorptivity at a given temperature [98]. This means that a perfectly absorbing metamaterial or metasurface may act as a great thermal emitter, or else, due to its thermal activity, it may act as an insulator or bolometer.

Bottom-up colloidal metasurfaces may also play a role in this field, since the metasurface inherits its property from the properties of meta-atoms. Film-coupled metasurfaces acting as

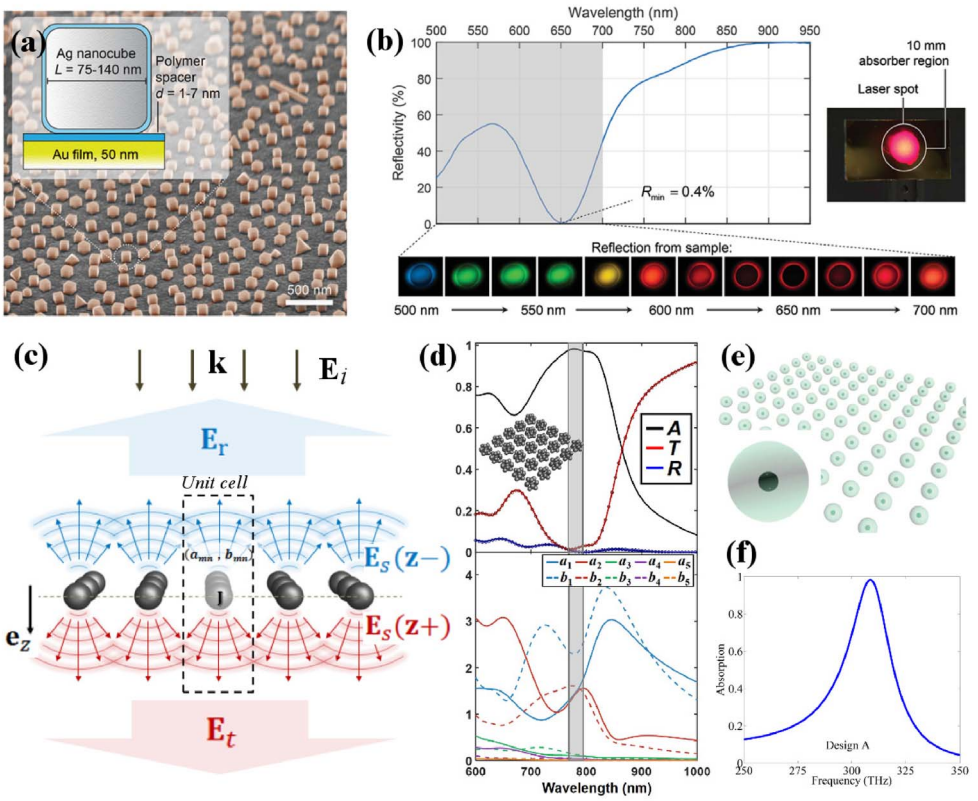

Figure 12. Nanocolloidal Perfect Absorbers. (a) Perfect absorbing metasurface composed of film coupled silver nanocubes ranging from 75 to 140 nm in size deposited on a gold evaporated film and spaced a few nanometers above the gold film. (b) Wavelength-dependence of the reflectivity exhibiting a resonant dip at $\lambda \approx 650$ nm. The photograph on the right-hand side of the graph show that large areas can be covered. (c) Illustration of a canonical metasurface composed of nanocolloids. The metasurface inherits its radiation properties from the scattering properties of the multipoles of the colloids. (d) Top graph: absorption (black), transmisttance (blue) and reflectance (red) spectrum of a perfect absorber composed of a periodic array of germanium nanoclusters. Bottom-graph: multipolar decomposition of the nanocluster in the array. (e) Metasurface composed of core-shell nanocolloids containing a silver core and a n-doped silicon shell. (f) Absorption spectrum of the core-shell metasurface. (a) and (b) are adapted from [102]. (c) and (d) are adapted from [103]. (e) and (f) are adapted from [104].

perfect absorbers have been demonstrated by Moreau *et al.* [99]. They are composed of silver nanocubes deposited on gold films with a separating dielectric gap layer of a couple of nanometers typically. The gap layer is composed of alternating positively and negatively charged polyelectrolytes deposited on the gold surface by dip-coating. The surfaces operate in reflectance and exhibit a resonance dip in the reflectance at a wavelength that is determined by the nanocube size and gap thickness. The amplitude of the resonance is governed by the surface fill fraction [100, 101]. Akselrod *et al.* have shown that such perfect absorbers could cover and conform to large areas (see Figure 12 (a,b)) [102].

Alternatively, it is also possible to produce perfect absorbers, that operate as transmissive monolayers of nanocolloids resonantly absorbing all the impinging light. For instance, a design was proposed by Radi *et al.* consisting in a periodic square array composed of core-shell nanocolloids containing a silver core and a n-doped silicon shell [104] (see Figure 12 (e)). These systems may resonantly act as Huygens dipoles (see Section 4.2), which ensures that no reflection from the metasurface occurs. Furthermore, they show that the perfect absorption condition is reached when both the electric and magnetic polarizabilities (α_e and α_m respectively) of the core-shell in the metasurface satisfies the following relation

$$\frac{\mu_0}{\varepsilon_0}\alpha_e = \frac{\varepsilon_0}{\mu_0}\alpha_m = \mathrm{i}\frac{S}{\omega} \tag{4}$$

where S is the area of the unit cell of the periodic array and μ_0 is the free-space magnetic permittivity. Figure 12 (f) shows that unity absorption is achieved for this system near a frequency equal to 300 THz.

It was shown recently by Dezert *et al.* that the nanocolloids do not have to be dipolar and that multipolar systems can be used in a periodic array to achieve perfect absorbtion (see Figure 12 (c)) [103]. Indeed, what is required is (i) that the sum of odd multipole modes be equal to the sum of even multipole modes, which is a generalization of the famous first Kerker condition (see Section 4.2) and produces Huygens multipoles (i.e. no back-scattering) and (ii) that they both be real and equal to a specific value such that zero-transmission occurs. The condition is summarized by the following relation

$$\sum_{n=1}^{\infty} \mathscr{O}_n = \sum_{n=1}^{\infty} \mathscr{E}_n = \frac{k^2 S}{\pi} \tag{5}$$

where $\mathscr{O}_n$ ($\mathscr{E}_n$) is the nth order odd (even) multipole and k is the free-space wavevector. This property, will ensure that the field radiated by all mutipoles will interfere destructively in the backward direction and reflectance will be cancelled. As a result of this generalization, several designs of perfect absorbing metasurfaces can be proposed. Figure 12 (d) provides an example where near unity absorption is achieved at optical wavelengths, with an array composed of germanium nanoclusters, which operate in a severely multipolar regime.

These designs have great potential for bottom-up nanocolloidal metasurfaces operating at optical frequencies.

5. Conclusion

The examples given in this review illustrate some advantages of the bottom-up approach over top-down fabrication routes for the realization of metamaterials operating in visible light. The extreme versatility of nanochemistry enables the large-scale synthesis of finely engineered meta-atoms. Moreover, self-assembly, relying solely on colloidal interactions, or directed-assembly, benefiting from external guiding constraints, enable the fabrication of bulk materials at little energy cost. In this way, assembling more than 10^9 meta-atoms in a volume of 10^6 μm^3 is routinely achieved. The successful observation of an isotropic effective magnetic permeability different from the vacuum value μ_0 in an optically thick metamaterial follows from this ability to produce and assemble a large number of resonators.

Bottom-up metamaterials nevertheless face many difficult challenges. Nanochemistry and self-assembly result in statistical distributions of the shape, size and ordering of the meta-atoms. For optical functions requiring a high precision in the response and the location of each meta-atom, like planar lenses, some top-down fabrication processes seem inescapable. On the other hand, if homogeneous effective optical properties are sought for, some degree of structural disorder at scales shorter than the wavelength has little impact. The random packing

of the magnetic meta-atoms is even necessary to enable the validity of an effective magnetic permeability parameter [14].

Increasing the optical response of the meta-atoms is another important challenge. In particular, higher values of their magnetic polarizability are needed for the production of Huygens metasurfaces or mu-near-zero (MNZ) materials. Silver has proved to be more efficient than gold in the raspberry model [14,62]. Mie-resonators made of high-index dielectric seem particularly promising for future materials [32, 105]. Increasing the magnetic response of the meta-atoms may however affect the validity of the permeability parameter μ and stimulate more theoretical work. Indeed, artificial magnetism is an effect of spatial dispersion of the permittivity that cannot in principle be reduced to a second-rank tensor μ_{ij} [106].

Optical losses constitute a major limitation for most applications of metamaterials in optics. Compensation of losses by addition of a gain medium excited by optical pumping is a complex and costly process that may be reserved for research studies or specific applications. The impact of losses can nevertheless be limited by using dielectric instead of plasmonic resonators or by reducing the optical thickness in metasurfaces. On the other hand, the Ohmic losses of plasmonic resonators are welcome for applications requiring a local source of heat like heat therapy.

Acknowledgements

The authors acknowledge support from the LabEx AMADEus (ANR-10-LABX-42) in the framework of IdExBordeaux (ANR-10-IDEX-03-02).

References

[1] V. Veselago, "Electrodynamics of substances with simultaneously negative electrical and magnetic permeabilities", *Phys.-Usp.* **10** (1968), no. 4, p. 504-509.
[2] C. R. Simovski, S. A. Tretyakov, "Historical notes on metamaterials", in *Theory and Phenomena of Metamaterials* (F. Capolino, ed.), vol. 1, CRC Press, 2009.
[3] N. Engheta, R. W. Ziolkowski, "Introduction, history, and selected topics in fundamental theories of metamaterials", in *Metamaterials* (N. Engheta, R. Ziolkowski, eds.), IEEE Press, 2006.
[4] A. I. Iyer, G. V. Eleftheriades, "Negative-refractive-index transmission-line metamaterials", in *Negative-Refracton Metamaterials* (G. V. Eleftheriades, K. G. Balmain, eds.), Wiley and Sons, 2005.
[5] C. M. Soukoulis, M. Wegener, "Past achievements and future challenges in the development of three-dimensional photonic metamaterials", *Nat. Photon.* **5** (2011), no. 9, p. 523.
[6] V. Ponsinet, A. Aradian, P. Barois, S. Ravaine, "Self-assembly and nanochemistry techniques for the fabrication of metamaterials", in *Theory and Phenomena of Metamaterials* (F. Capolino, ed.), vol. 2, CRC Press, 2009.
[7] A. Baron, A. Aradian, V. Ponsinet, P. Barois, "Self-assembled optical metamaterials", *Opt. Laser Technol.* **82** (2016), p. 94-100.
[8] V. Ponsinet, A. Baron, E. Pouget, Y. Okazaki, R. Oda, P. Barois, "Self-assembled nanostructured metamaterials", *Europhys. Lett.* **119** (2017), no. 1, article ID 14004.
[9] J. C. Berg, *An Introduction to Interfaces and Colloids: The Bridge to Nanoscience*, World Scientific, 2010.
[10] T. Cosgrove, *Colloid Science: Principles, Methods and Applications*, Wiley and Sons, 2010.
[11] M. Lahmani, C. Bréchignac, P. Houdy, "Les nanosciences", in *Nanomateriaux et nanochimie*, vol. 2, Belin, 2006.
[12] C. Bréchignac, P. Houdy, M. Lahmani, *Nanomaterials and Nanochemistry*, Springer, 2007.
[13] A. Baron, A. Iazzolino, K. Ehrhardt, J.-B. Salmon, A. Aradian, V. Kravets, A. N. Grigorenko, J. Leng, A. Le Beulze, M. Tréguer-Delapierre *et al.*, "Bulk optical metamaterials assembled by microfluidic evaporation", *Opt. Mater. Express* **3** (2013), no. 11, p. 1792-1797.
[14] S. Gomez-Graña, A. Le Beulze, M. Treguer-Delapierre, S. Mornet, E. Duguet, E. Grana, E. Cloutet, G. Hadziioannou, J. Leng, J.-B. Salmon *et al.*, "Hierarchical self-assembly of a bulk metamaterial enables isotropic magnetic permeability at optical frequencies", *Mater. Horiz.* **3** (2016), no. 6, p. 596-601.
[15] X. Fan, W. Zheng, D. J. Singh, "Light scattering and surface plasmons on small spherical particles", *Light: Sci. Appl.* **3** (2014), no. 6, article ID e179–e179.
[16] S. Gwo, H.-Y. Chen, M.-H. Lin, L. Sun, X. Li, "Nanomanipulation and controlled self-assembly of metal nanoparticles and nanocrystals for plasmonics", *Chem. Soc. Rev.* **45** (2016), no. 20, p. 5672-5716.

[17] J. B. Pendry, "Negative refraction makes a perfect lens", *Phys. Rev. Lett.* **85** (2000), no. 18, p. 3966.
[18] J. B. Pendry, D. Schurig, D. R. Smith, "Controlling electromagnetic fields", *Science* **312** (2006), no. 5781, p. 1780-1782.
[19] V. M. Shalaev, "Transforming light", *Science* **322** (2008), no. 5900, p. 384-386.
[20] L. D. Landau, J. Bell, M. Kearsley, L. Pitaevskii, E. Lifshitz, J. Sykes, *Electrodynamics of Continuous Media, Vol. 8*, Elsevier, 2013.
[21] J. B. Pendry, A. J. Holden, D. J. Robbins, W. Stewart *et al.*, "Magnetism from conductors and enhanced nonlinear phenomena", *IEEE Trans. Microw. Theory Tech.* **47** (1999), no. 11, p. 2075-2084.
[22] R. A. Shelby, D. R. Smith, S. Schultz, "Experimental verification of a negative index of refraction", *Science* **292** (2001), no. 5514, p. 77-79.
[23] A. Alù, A. Salandrino, N. Engheta, "Negative effective permeability and left-handed materials at optical frequencies", *Opt. Express* **14** (2006), no. 4, p. 1557-1567.
[24] A. Alu, N. Engheta, "The quest for magnetic plasmons at optical frequencies", *Opt. Express* **17** (2009), no. 7, p. 5723-5730.
[25] C. Simovski, S. Tretyakov, "Model of isotropic resonant magnetism in the visible range based on core-shell clusters", *Phys. Rev. B* **79** (2009), no. 4, article ID 045111.
[26] J. Lekner, "Optical properties of isotropic chiral media", *Pure Appl. Opt.: J. Eur. Opt. Soc. A* **5** (1996), no. 4, p. 417.
[27] A. Kuzyk, R. Schreiber, Z. Fan, G. Pardatscher, E.-M. Roller, A. Högele, F. C. Simmel, A. O. Govorov, T. Liedl, "DNA-based self-assembly of chiral plasmonic nanostructures with tailored optical response", *Nature* **483** (2012), no. 7389, p. 311.
[28] X. Fu, Y. Wang, L. Huang, Y. Sha, L. Gui, L. Lai, Y. Tang, "Assemblies of metal nanoparticles and self-assembled peptide fibrils—formation of double helical and single-chain arrays of metal nanoparticles", *Adv. Mater.* **15** (2003), no. 11, p. 902-906.
[29] J. Cheng, G. Le Saux, J. Gao, T. Buffeteau, Y. Battie, P. Barois, V. Ponsinet, M.-H. Delville, O. Ersen, E. Pouget *et al.*, "Goldhelix: gold nanoparticles forming 3d helical superstructures with controlled morphology and strong chiroptical property", *ACS Nano* **11** (2017), no. 4, p. 3806-3818.
[30] A. Vallecchi, M. Albani, F. Capolino, "Collective electric and magnetic plasmonic resonances in spherical nanoclusters", *Opt. Express* **19** (2011), no. 3, p. 2754-2772.
[31] V. Giannini, A. I. Fernández-Domínguez, S. C. Heck, S. A. Maier, "Plasmonic nanoantennas: fundamentals and their use in controlling the radiative properties of nanoemitters", *Chem. Rev.* **111** (2011), no. 6, p. 3888-3912.
[32] S. Jahani, Z. Jacob, "All-dielectric metamaterials", *Nat. Nanotechnol.* **11** (2016), no. 1, p. 23.
[33] J. Valentine, J. Li, T. Zentgraf, G. Bartal, X. Zhang, "An optical cloak made of dielectrics", *Nat. Mater.* **8** (2009), no. 7, p. 568.
[34] M. Khorasaninejad, W. T. Chen, R. C. Devlin, J. Oh, A. Y. Zhu, F. Capasso, "Metalenses at visible wavelengths: diffraction-limited focusing and subwavelength resolution imaging", *Science* **352** (2016), no. 6290, p. 1190-1194.
[35] A. B. Evlyukhin, S. M. Novikov, U. Zywietz, R. L. Eriksen, C. Reinhardt, S. I. Bozhevolnyi, B. N. Chichkov, "Demonstration of magnetic dipole resonances of dielectric nanospheres in the visible region", *Nano Lett.* **12** (2012), no. 7, p. 3749-3755.
[36] S. Zhang, R. Jiang, Y.-M. Xie, Q. Ruan, B. Yang, J. Wang, H.-Q. Lin, "Colloidal moderate-refractive-index Cu_2O nanospheres as visible-region nanoantennas with electromagnetic resonance and directional light-scattering properties", *Adv. Mater.* **27** (2015), no. 45, p. 7432-7439.
[37] R. Dezert, P. Richetti, A. Baron, "Isotropic Huygens dipoles and multipoles with colloidal particles", *Phys. Rev. B* **96** (2017), no. 18, article ID 180201.
[38] F. Timpu, A. Sergeyev, N. R. Hendricks, R. Grange, "Second-harmonic enhancement with Mie resonances in perovskite nanoparticles", *ACS Photon.* **4** (2016), no. 1, p. 76-84.
[39] A. L. Lereu, R. Farahi, L. Tetard, S. Enoch, T. Thundat, A. Passian, "Plasmon assisted thermal modulation in nanoparticles", *Opt. Express* **21** (2013), no. 10, p. 12145-12158.
[40] P. Berini, I. De Leon, "Surface plasmon-polariton amplifiers and lasers", *Nat. Photon.* **6** (2011), p. 16-24.
[41] O. Hess, J. B. Pendry, S. Maier, R. Oulton, J. Hamm, K. Tsakmakidis, "Active nanoplasmonic metamaterials", *Nat. Mater.* **11** (2012), p. 573-584.
[42] K. F. MacDonald, N. I. Zheludev, "Active plasmonics: current status", *Laser Photon. Rev.* **4** (2010), no. 4, p. 562-567.
[43] M. Noginov, G. Zhu, M. Bahoura, J. Adegoke, C. Small, B. Ritzo, V. Drachev, V. Shalaev, "The effect of gain and absorption on surface plasmons in metal nanoparticles", *Appl. Phys. B* **86** (2007), no. 3, p. 455-460.
[44] A. De Luca, M. P. Grzelczak, I. Pastoriza-Santos, L. M. Liz-Marzán, M. La Deda, M. Striccoli, G. Strangi, "Dispersed and encapsulated gain medium in plasmonic nanoparticles: a multipronged approach to mitigate optical losses", *ACS Nano* **5** (2011), no. 7, p. 5823-5829.
[45] A. De Luca, M. Ferrie, S. Ravaine, M. La Deda, M. Infusino, A. R. Rashed, A. Veltri, A. Aradian, N. Scaramuzza, G. Strangi, "Gain functionalized core–shell nanoparticles: the way to selectively compensate absorptive losses", *J. Mater. Chem.* **2** (2012), p. 8846-8852.
[46] R.-M. Ma, R. F. Oulton, "Applications of nanolasers", *Nat. Nanotechnol.* **14** (2019), p. 12-22.

[47] Z. Wang, X. Meng, A. V. Kildishev, A. Boltasseva, V. M. Shalaev, "Nanolasers enabled by metallic nanoparticles: from spasers to random lasers", *Laser Photon. Rev.* **11** (2017), no. 6, article ID 1700212.
[48] M. Noginov, G. Zhu, A. Belgrave, R. Bakker, V. M. Shalaev, E. Narimanov, S. Stout, E. Herz, T. Suteewong, U. Wiesner, "Demonstration of a spaser-based nanolaser", *Nature* **460** (2009), p. 1110-1112.
[49] X. Meng, A. V. Kildishev, K. Fujita, K. Tanaka, V. M. Shalaev, "Wavelength-tunable spasing in the visible", *Nano Lett.* **13** (2013), no. 9, p. 4106-4112.
[50] A. Veltri, A. Aradian, "Optical response of a metallic nanoparticle immersed in a medium with optical gain", *Phys. Rev. B* **85** (2012), no. 11, article ID 115429.
[51] V. Pustovit, F. Capolino, A. Aradian, "Cooperative plasmon-mediated effects and loss compensation by gain dyes near a metal nanoparticle", *J. Opt. Soc. Am. B* **32** (2015), no. 02, p. 188-193.
[52] A. Veltri, A. Chipouline, A. Aradian, "Multipolar, time-dynamical model for the loss compensation and lasing of a spherical plasmonic nanoparticle spaser immersed in an active gain medium", *Sci. Rep.* **6** (2016), p. 33018.
[53] A. Veltri, K. Caicedo, A. Cathey, A. Aradian, to be published (2019).
[54] J. Vieaud, O. Merchiers, M. Rajaoarivelo, M. Warenghem, Y. Borensztein, V. Ponsinet, A. Aradian, "Effective medium description of plasmonic couplings in disordered polymer and gold nanoparticle composites", *Thin Solid Films* **603** (2016), p. 452-464.
[55] L. Malassis, P. Massé, M. Tréguer-Delapierre, S. Mornet, P. Weisbecker, V. Kravets, A. Grigorenko, P. Barois, "Bottom-up fabrication and optical characterization of dense films of meta-atoms made of core–shell plasmonic nanoparticles", *Langmuir* **29** (2013), no. 5, p. 1551-1561.
[56] V. Kravets, F. Schedin, R. Jalil, L. Britnell, R. Gorbachev, D. Ansell, B. Thackray, K. Novoselov, A. Geim, A. V. Kabashin *et al.*, "Singular phase nano-optics in plasmonic metamaterials for label-free single-molecule detection", *Nat. Mater.* **12** (2013), no. 4, p. 304.
[57] C. Coutant, S. Ravaine, X. Wang, J. Toudert, V. Ponsinet, P. Barois, "Plasmonic metamaterials for ultra-sensitive sensing: topological darkness", *Rend. Lincei* **26** (2015), no. 2, p. 175-182.
[58] F. Aubrit, F. Testard, A. Paquirissamy, F. Gobeaux, X. Wang, F. Nallet, P. Fontaine, V. Ponsinet, P. Guenoun, "Ligand-free synthesis of gold nanoparticles incorporated within cylindrical block copolymer films", *J. Mater. Chem. C* **6** (2018), no. 30, p. 8194-8204.
[59] J. Toudert, X. Wang, C. Tallet, P. Barois, A. Aradian, V. Ponsinet, "Plasmonic optical interferences for phase-monitored nanoscale sensing in low-loss three-dimensional metamaterials", *ACS Photon.* **2** (2015), no. 10, p. 1443-1450.
[60] A. Grigorenko, P. Nikitin, A. Kabashin, "Phase jumps and interferometric surface plasmon resonance imaging", *Appl. Phys. Lett.* **75** (1999), no. 25, p. 3917-3919.
[61] K. Johansen, R. Stålberg, I. Lundström, B. Liedberg, "Surface plasmon resonance: instrumental resolution using photo diode arrays", *Meas. Sci. Technol.* **11** (2000), no. 11, p. 1630.
[62] V. Ponsinet, P. Barois, S. M. Gali, P. Richetti, J.-B. Salmon, A. Vallecchi, M. Albani, A. Le Beulze, S. Gomez-Grana, E. Duguet *et al.*, "Resonant isotropic optical magnetism of plasmonic nanoclusters in visible light", *Phys. Rev. B* **92** (2015), no. 22, article ID 220414.
[63] J. Angly, A. Iazzolino, J.-B. Salmon, J. Leng, S. P. Chandran, V. Ponsinet, A. Désert, A. Le Beulze, S. Mornet, M. Tréguer-Delapierre *et al.*, "Microfluidic-induced growth and shape-up of three-dimensional extended arrays of densely packed nanoparticles", *ACS Nano* **7** (2013), no. 8, p. 6465-6477.
[64] V. Kravets, O. Marshall, R. Nair, B. Thackray, A. Zhukov, J. Leng, A. Grigorenko, "Engineering optical properties of a graphene oxide metamaterial assembled in microfluidic channels", *Opt. Express* **23** (2015), no. 2, p. 1265-1275.
[65] Q. Flamant, D. Torrent, S. Gomez-Graña, A. N. Grigorenko, V. G. Kravets, P. Barois, V. Ponsinet, A. Baron, "Direct retrieval method of the effective permittivity and permeability of bulk semi-infinite metamaterials by variable-angle spectroscopic ellipsometry", *OSA Contin.* **2** (2019), no. 5, p. 1762-1772.
[66] X. Wang, K. Ehrhardt, C. Tallet, M. Warenghem, A. Baron, A. Aradian, M. Kildemo, V. Ponsinet, "Hyperbolic-by-design self-assembled metamaterial based on block copolymers lamellar phases", *Opt. Laser Technol.* **88** (2017), p. 85-95.
[67] L. Ferrari, C. Wu, D. Lepage, X. Zhang, Z. Liu, "Hyperbolic metamaterials and their applications", *Prog. Quantum Electron.* **40** (2015), p. 1-40.
[68] A. Poddubny, I. Iorsh, P. Belov, Y. Kivshar, "Hyperbolic metamaterials", *Nat. Photon.* **7** (2013), no. 12, p. 948.
[69] Y. Guo, W. Newman, C. L. Cortes, Z. Jacob, "Applications of hyperbolic metamaterial substrates", *Adv. OptoElectron.* **2012** (2012), article ID 452502.
[70] I. I. Smolyaninov, V. N. Smolyaninova, "Hyperbolic metamaterials: novel physics and applications", *Solid-State Electron.* **136** (2017), p. 102-112.
[71] J. Yao, Z. Liu, Y. Liu, Y. Wang, C. Sun, G. Bartal, A. M. Stacy, X. Zhang, "Optical negative refraction in bulk metamaterials of nanowires", *Science* **321** (2008), no. 5891, p. 930-930.
[72] N. A. Melosh, A. Boukai, F. Diana, B. Gerardot, A. Badolato, P. M. Petroff, J. R. Heath, "Ultrahigh-density nanowire lattices and circuits", *Science* **300** (2003), no. 5616, p. 112-115.

[73] W. M. Gelbart, A. Ben-Shaul, D. Roux, *Micelles, Membranes, Microemulsions, and Monolayers*, Springer Science & Business Media, 2012.
[74] P.-G. De Gennes, J. Prost, *The Physics of Liquid Crystals, Vol. 83*, Oxford University Press, 1995.
[75] T. P. Lodge, "Block copolymers: past successes and future challenges", *Macromol. Chem. Phys.* **204** (2003), no. 2, p. 265-273.
[76] Y. Gao, J. Huang, Y. Liu, L. Gao, K. Yu, X. Zhang, "Optical negative refraction in ferrofluids with magnetocontrollability", *Phys. Rev. Lett.* **104** (2010), no. 3, article ID 034501.
[77] V. N. Smolyaninova, B. Yost, D. Lahneman, E. E. Narimanov, I. I. Smolyaninov, "Self-assembled tunable photonic hyper-crystals", *Sci. Rep.* **4** (2014), p. 5706.
[78] J. A. Roberts, S.-J. Yu, P.-H. Ho, S. Schoeche, A. L. Falk, J. A. Fan, "Tunable hyperbolic metamaterials based on self-assembled carbon nanotubes", *Nano Lett.* **19** (2019), no. 5, p. 3131-3137.
[79] I. W. Hamley, *The Physics of Block Copolymers, Vol. 19*, Oxford University Press, Oxford, 1998.
[80] S. B. Glybovski, S. A. Tretyakov, P. A. Belov, Y. S. Kivshar, C. R. Simovski, "Metasurfaces: from microwaves to visible", *Phys. Rep.* **634** (2016), p. 1-72.
[81] P. Jacquet, B. Bouteille, R. Dezert, J. Lautru, R. Podor, A. Baron, J. Teisseire, J. Jupille, R. Lazzari, I. Gozhyk, "Periodic arrays of diamond-shaped silver nanoparticles: from scalable fabrication by template-assisted solid-state dewetting to tunable optical properties", *Adv. Funct. Mater.* (2019), article ID 1901119.
[82] Y. Cui, M. T. Björk, J. A. Liddle, C. Sönnichsen, B. Boussert, A. P. Alivisatos, "Integration of colloidal nanocrystals into lithographically patterned devices", *Nano Lett.* **4** (2004), no. 6, p. 1093-1098.
[83] C. Kuemin, L. Nowack, L. Bozano, N. D. Spencer, H. Wolf, "Oriented assembly of gold nanorods on the single-particle level", *Adv. Funct. Mater.* **22** (2012), no. 4, p. 702-708.
[84] Z. Liu, T. Chang, H. Huang, T. He, "Gold nanoparticle arrays assembled on the reconstructed surface of block copolymer thin films", *RSC Adv.* **3** (2013), no. 43, p. 20464-20470.
[85] K. Aissou, M. Mumtaz, A. Alvarez-Fernandez, J. Mercat, S. Antoine, G. Pécastaings, V. Ponsinet, C. Dobrzynski, G. Fleury, G. Hadziioannou, "Metallic nanodot patterns with unique symmetries templated from ABC triblock terpolymer networks", *Macromol. Rapid Commun.* **39** (2018), no. 7, article ID 1700754.
[86] A. Alvarez-Fernandez, K. Aissou, G. Pécastaings, G. Hadziioannou, G. Fleury, V. Ponsinet, "High refractive index in low metal content nanoplasmonic surfaces from self-assembled block copolymer thin films", *Nanoscale Adv.* **1** (2019), no. 2, p. 849-857.
[87] J. Chai, D. Wang, X. Fan, J. M. Buriak, "Assembly of aligned linear metallic patterns on silicon", *Nat. Nanotechnol.* **2** (2007), no. 8, p. 500.
[88] Q. Peng, Y.-C. Tseng, S. B. Darling, J. W. Elam, "Nanoscopic patterned materials with tunable dimensions via atomic layer deposition on block copolymers", *Adv. Mater.* **22** (2010), no. 45, p. 5129-5133.
[89] R. Ruiz, H. Kang, F. A. Detcheverry, E. Dobisz, D. S. Kercher, T. R. Albrecht, J. J. de Pablo, P. F. Nealey, "Density multiplication and improved lithography by directed block copolymer assembly", *Science* **321** (2008), no. 5891, p. 936-939.
[90] C. Cummins, T. Ghoshal, J. D. Holmes, M. A. Morris, "Strategies for inorganic incorporation using neat block copolymer thin films for etch mask function and nanotechnological application", *Adv. Mater.* **28** (2016), no. 27, p. 5586-5618.
[91] M. Haarmans, D. Bedeaux, "Optical properties of thin films up to second order in the thickness", *Thin Solid Films* **258** (1995), no. 1–2, p. 213-223.
[92] A. Alvarez-Fernandez, G. Fleury, V. Ponsinet, P. M. Walmsness, M. Kildemo, "Formation and optical response of self-assembled gold nanoparticle lattices on oxidized silicon synthesized using block copolymers", *J. Vac. Sci. Technol. B* **38** (2020), no. 1, article ID 013601.
[93] A. Arbabi, Y. Horie, M. Bagheri, A. Faraon, "Dielectric metasurfaces for complete control of phase and polarization with subwavelength spatial resolution and high transmission", *Nat. Nanotechnol.* **10** (2015), no. 11, p. 937.
[94] M. Kerker, D.-S. Wang, C. Giles, "Electromagnetic scattering by magnetic spheres", *JOSA* **73** (1983), no. 6, p. 765-767.
[95] C. Huygens, *Traité de la lumière*, Gauthier-Villars, 1920, 174 pages.
[96] M. Decker, I. Staude, M. Falkner, J. Dominguez, D. N. Neshev, I. Brener, T. Pertsch, Y. S. Kivshar, "High-efficiency dielectric Huygens' surfaces", *Adv. Opt. Mater.* **3** (2015), no. 6, p. 813-820.
[97] R. Dezert, P. Richetti, A. Baron, "Isotropic Huygens sources made of clusters of nanoparticles for metasurfaces applications", *J. Phys.: Conf. Ser.* **1092** (2018), article ID 012022.
[98] G. Kirchhoff, "Ueber das verhältniss zwischen dem emissionsvermögen und dem absorptionsvermögen der körper für wärme und licht", *Ann. Phys.* **185** (1860), no. 2, p. 275-301.
[99] A. Moreau, C. Ciracì, J. J. Mock, R. T. Hill, Q. Wang, B. J. Wiley, A. Chilkoti, D. R. Smith, "Controlled-reflectance surfaces with film-coupled colloidal nanoantennas", *Nature* **492** (2012), no. 7427, p. 86.
[100] P. T. Bowen, A. Baron, D. R. Smith, "Theory of patch-antenna metamaterial perfect absorbers", *Phys. Rev. A* **93** (2016), no. 6, article ID 063849.

[101] P. Bowen, A. Baron, D. Smith, "Effective-medium description of a metasurface composed of a periodic array of nanoantennas coupled to a metallic film", *Phys. Rev. A* **95** (2017), no. 3, article ID 033822.
[102] G. M. Akselrod, J. Huang, T. B. Hoang, P. T. Bowen, L. Su, D. R. Smith, M. H. Mikkelsen, "Large-area metasurface perfect absorbers from visible to near-infrared", *Adv. Mater.* **27** (2015), no. 48, p. 8028-8034.
[103] R. Dezert, P. Richetti, A. Baron, "Complete multipolar description of reflection and transmission across a metasurface for perfect absorption of light", *Opt. Exp.* **27** (2019), p. 26317-26330.
[104] Y. Ra'di, V. S. Asadchy, S. U. Kosulnikov, M. M. Omelyanovich, D. Morits, A. V. Osipov, C. R. Simovski, S. A. Tretyakov, "Full light absorption in single arrays of spherical nanoparticles", *ACS Photon.* **2** (2015), no. 5, p. 653-660.
[105] M. L. De Marco, S. Semlali, B. A. Korgel, P. Barois, G. L. Drisko, C. Aymonier, "Silicon-based dielectric metamaterials: focus on the current synthetic challenges", *Angew. Chem.* **57** (2018), p. 4478-4498.
[106] V. M. Agranovich, V. Ginzburg, *Crystal Optics with Spatial Dispersion, and Excitons*, Springer-Verlag, Berlin, Heidelberg GmbH, 1984.